ChemComm

COMMUNICATION

View Article Online
View Journal | View Issue

Cite this: *Chem. Commun.*, 2024, **60**, 13706

Received 27th August 2024,
Accepted 25th October 2024

DOI: 10.1039/d4cc04381b

rsc.li/chemcomm

Synthesis of battery-grade $FePO_4{\cdot}2H_2O$ using high-pressure hydrolyzed precipitates of cobalt–iron alloy acid solution†

Xuan Du,[a] Zhanhong Wang,*[b] Bin Zheng,[b] Shanlin Shi,[c] Wei Xu,[b] Shuo Wang,[b] Peng Shi,[a] Tao Zhou[a] and Guo Gao *[a]

Herein, we developed a facile method for the synthesis of battery-grade ferric phosphate ($FePO_4{\cdot}2H_2O$) using high-pressure hydrolyzed precipitates of cobalt–iron alloy acid solution. The size of the prepared $FePO_4{\cdot}2H_2O$ samples was about 5–10 μm, and the microstructure of $FePO_4{\cdot}2H_2O$ was polyhedral. The $FePO_4{\cdot}2H_2O$ samples exhibited a high Fe/P ratio (1.03) compared with standard ferric phosphate (0.98–1.02), indicating potentially good electrochemical performance. The significance of the current work is that we have developed an effective method for the resource utilization of solid waste containing iron.

In the past few years, the demand for raw materials for energy has increased sharply with the rapid worldwide development of new energy vehicles.[1–3] Lithium iron phosphate ($LiFePO_4$) batteries show better safety performance than ternary materials. The thermal decomposition temperature of $LiFePO_4$ is about 700 °C, and the thermal decomposition temperature of a ternary material is 200–300 °C. $LiFePO_4$ can maintain a more stable structure even at high temperature, which makes an $LiFePO_4$ battery much safer and more reliable. As an important raw material of $LiFePO_4$ positive materials, the raw material of ferric phosphate ($FePO_4$) has attracted a lot of attention.[4–6] Wang *et al.* reported $FePO_4{\cdot}2H_2O$ nanoplates for the high-rate performance of $LiFePO_4$ materials.[7] When the surface of $FePO_4{\cdot}2H_2O$ nanoplates was coated by a carbon layer, the hybrid materials exhibited 75 mA h g^{-1} even at a rate of 30C. Generally, the synthesis of $FePO_4$ mainly includes the sodium process, ammonium process and iron powder process.[8,9] As for the sodium process of $FePO_4$, the $FeSO_4$ solution was acidized with H_3PO_4 and then reacted with H_2O_2 to produce ferric dihydrogen phosphate, and the solution pH value was adjusted to ~2.0 to produce $FePO_4$. As for the ammonium process, the $FeSO_4$ solution was reacted with monoammonium phosphate. After precipitation and filtration, the excess acid was neutralized by ammonia water, then $FePO_4$ was obtained. As for the iron powder process, the iron powder was reacted with H_3PO_4 solution. The main advantages of this method are less wastage of water and less environmental contamination, but the main problems are hydrogen emission and high cost.

Against the background of the vigorous development of the global battery industry and increasing attention to production costs, the use of industrial waste liquid containing iron ions to prepare battery-grade $FePO_4$ has shown great potential.[10,11] Deng *et al.* reported a liquid-phase method for the synthesis of $FePO_4$ battery materials using industrial $FeSO_4$ solution from acid processed titanium dioxide.[11] The use of industrial waste liquid containing iron ions to prepare $FePO_4$ has the following advantages: (1) the cost of the industrial $FeSO_4$ solution is very low, and some industries can even provide $FeSO_4$ without any cost. However, iron powder is high cost; (2) the abundant hydrogen produced from the iron powder process for $FePO_4$ poses a huge security risk. Cobalt iron alloy comes mainly from the copper smelting of cobalt-containing slag, where cobalt iron alloy contains a lot of iron and a small amount of cobalt.[12] After sulfuric acid leaching treatment of cobalt iron alloy, a small amount of cobalt element is extracted, and a large number of iron elements exist in the liquid solution; iron in the solution is mainly in the form of $FeSO_4$, which contains lots of impurities (Al, Cr, Ca, Zn *etc.*). The high-pressure hydrolyzed precipitate of cobalt–iron alloy acid solution is a typical solid waste containing iron. The use of high-pressure hydrolyzed precipitate to prepare battery-grade $FePO_4$ will be investigated in this work.

Typically, 2 g of high-pressure hydrolyzed precipitates of cobalt–iron alloy acid solution were dispersed in deionized water, and the high-pressure hydrolyzed precipitates were dissolved using dilute phosphoric acid solution at an elevated

[a] *School of Sensing Science and Engineering, School of Electronic Information and Electrical Engineering, Shanghai Jiao Tong University, Shanghai 200240, China. E-mail: guogao@sjtu.edu.cn*
[b] *China Nonferrous Metals Innovation Institute (Tianjin) Co., Ltd., Tianjin 300393, China. E-mail: Wangzhh@otic.com.cn*
[c] *Shenyang Nonferrous Metals Research Institute Co., Ltd, Shenyang 110141, China*

† Electronic supplementary information (ESI) available. See DOI: https://doi.org/10.1039/d4cc04381b

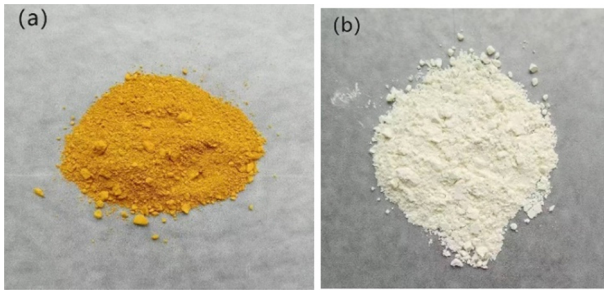

Fig. 1 Optical photographs of the high-pressure hydrolyzed precipitates (a), and the synthesized $FePO_4{\cdot}2H_2O$ samples (b).

temperature (105 °C, in an oil bath). After the complete dissolution of high-pressure hydrolyzed precipitates, the mixed solution was cooled to room temperature. After that, some reduced iron powders were added into the mixed solution to consume the excess phosphoric acid, and then the pH value of the mixed solution was adjusted to 2.57 and a lot of white precipitates appeared. The white precipitates were elevated to 85 °C for 30 min, and then the precipitates were washed with dilute nitric acid and deionized water and centrifuged at 4000 rpm using a centrifugal machine. The obtained products were dried at 60 °C for 24 h, and then the composition and structure of the synthesized battery-grade $FePO_4$ were characterized by X-ray diffraction (XRD), scanning electron microscopy (SEM), transmission electron microscopy (TEM), X-ray photoelectron spectroscopy (XPS), thermos-gravimetric curve analysis (TGA) and X-ray fluorescence spectrometry (XRF).

The morphology of high-pressure hydrolyzed precipitates of cobalt–iron alloy acid solution is shown in Fig. 1(a). The colour of the high-pressure hydrolyzed precipitates is yellow. XRF measurement was used to analyze the composition of high-pressure hydrolyzed precipitates, which is shown in Table 1. It can clearly be seen that the amounts of impurity elements (Al, Cr, Ca, Zn *etc.*) are high. The synthesized battery-grade $FePO_4$ is shown in Fig. 1(b). The colour of $FePO_4$ was white. The inductively coupled plasma (ICP) analysis of the ferric phosphate products is shown in Table 2. From Table 2, it is evident that the impurity elements (Al, Cr, Ca, Zn *etc.*) can be effectively removed during the process of synthesizing ferric phosphate. This suggested that the contents of total Fe and P are 31.909% and 17.146%, respectively. The elements of Co, Cu, K, Mg, Mn and Na are not detected. The Fe/P ratio of the synthesized ferric phosphate products is 1.03, which is higher than that of standard HG/T4701-2021 ferric phosphate (0.98–1.02). This means the prepared $FePO_4$ product could act as a potential promising candidate material for $LiFePO_4$.

Table 2 ICP analysis of synthesized battery-grade $FePO_4{\cdot}2H_2O$

Element	Al	Ca	Co	Cr	Cu	Fe	K
Conc. unit	0.005%	0.007%	—	0.003%	—	31.909%	—

Element	Mg	Mn	Na	P	Pb	Ti	Zn
Conc. unit	—	—	—	17.146%	0.003%	0.022%	0.002%

The XRD analysis of the synthesized battery-grade ferric phosphate is shown in Fig. 2(a). The XRD pattern of the samples showed that the diffraction peaks of the materials were sharp, indicating that the samples had good crystallinity. The typical peaks of the samples were consistent with the crystalline $FePO_4{\cdot}2H_2O$ phases (JCPDS no. 29-0715).[13] The TGA measurement in Fig. 2(b) shows that the synthesized ferric phosphate samples have an evident weight loss at 200 °C, which is attributed to the removal of crystal water in ferric phosphate samples. Generally, the crystal water in the samples is more stable than the physically adsorbed water. It is clear that the synthesized ferric phosphate samples are stable up to 150 °C, and show about 19.25% weight loss at 200 °C. The TGA results confirm that the synthesized ferric phosphate has two crystal waters, that is, $FePO_4{\cdot}2H_2O$. The SEM image in Fig. 2(c) shows that the average particle size of synthesized $FePO_4{\cdot}2H_2O$ is 5–10 μm. The particle size is relatively dispersed, and there is no severe agglomeration phenomenon. Fig. 2(d) shows the high-magnification image of the samples. It shows that the surface of the $FePO_4{\cdot}2H_2O$ particle is smooth, and the boundary of the $FePO_4{\cdot}2H_2O$ particle is clear. Fig. 2e shows the TEM image of the synthesized $FePO_4{\cdot}2H_2O$ products. The $FePO_4{\cdot}2H_2O$ particle has a polyhedral structure, and the high-resolution TEM image (Fig. 2(f)) shows that the boundary of the $FePO_4{\cdot}2H_2O$ particle has a certain degree of crystallization, but the lattice fringe is hard to acquire because the size of the $FePO_4{\cdot}2H_2O$ particle is too big.

The XPS spectra of synthesized battery-grade $FePO_4{\cdot}2H_2O$ samples are shown in Fig. 3(a). The survey spectrum shows the presence of Fe, P and O elements, suggesting the successful synthesis of ferric phosphate. The peaks at 725.8 eV and 711.7 eV in the Fe 2p spectrum (Fig. 3(b)) indicate the presence of Fe(III), which is consistent with the reported data for $FePO_4$.[14,15] There is no Fe(II) peak, which should be at ~708.0 eV.[16] As for the P 2p spectrum (Fig. 3(c)), there is an evident spin–orbit doublet with a dominant peak at 133.3 eV,

Table 1 XRF analysis of high-pressure hydrolyzed precipitates

Comp.	Al_2O_3	SiO_2	SO_3	CaO	V_2O_5	Cr_2O_3	Fe_2O_3
Conc. unit	785.6 ppm	387.0 ppm	6.457%	0.118%	54.9 ppm	0.127%	85.957%

Comp.	NiO	ZnO	ZrO_2	MoO_3	Ag_2O	SnO_2	Bi_2O_3
Conc. unit	0.119%	403.2 ppm	224.8 ppm	9.3 ppm	0.140%	78.7 ppm	425.0 ppm

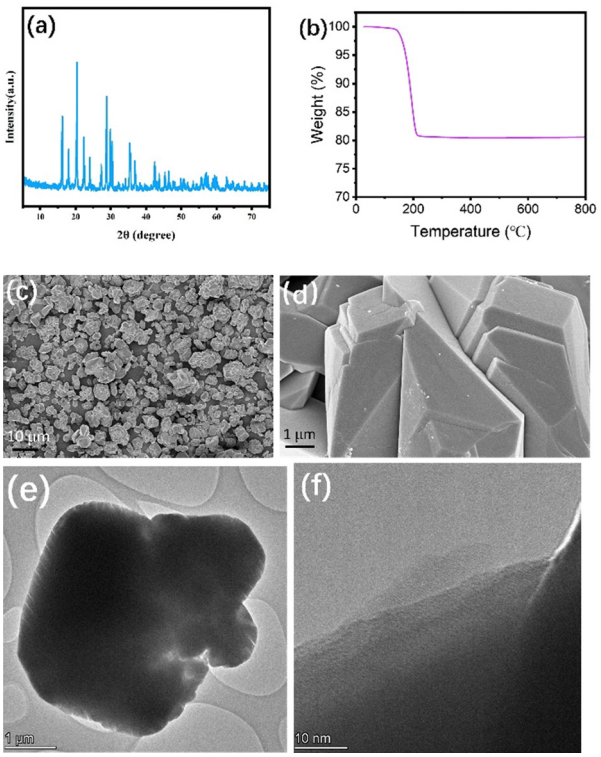

Fig. 2 XRD (a), TGA (b), SEM (c) and (d) and TEM (e) and (f) images of the synthesized battery-grade $FePO_4{\cdot}2H_2O$ samples.

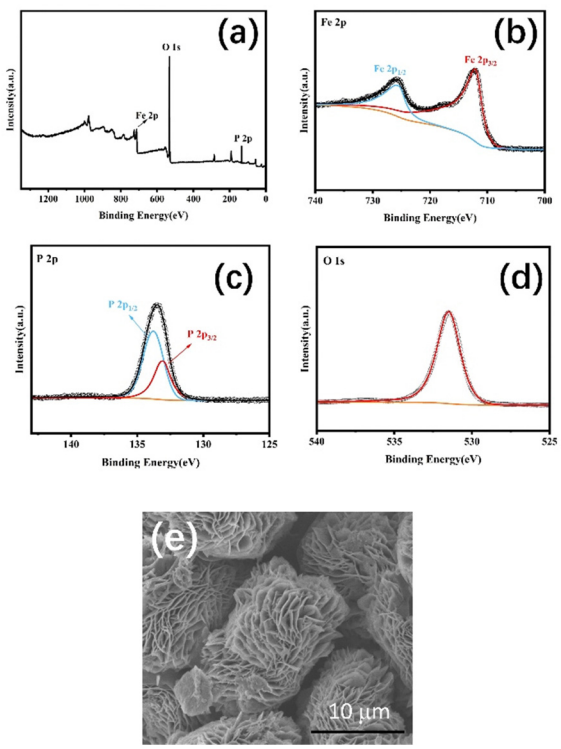

Fig. 3 XPS of the synthesized battery-grade $FePO_4{\cdot}2H_2O$ samples (a), Fe 2p (b), P 2p (c), O 1s (d) and the SEM of the prepared $FePO_4{\cdot}2H_2O$ samples in the absence of 85 °C heat treatment (e).

Table 3 ICP analysis of prepared $FePO_4{\cdot}2H_2O$ without acid washing

Element	Al	Ca	Co	Cr	Cu	Fe	K
Conc. unit	0.007%	0.006%	—	0.003%	—	30.477%	—

Element	Mg	Mn	Na	P	Pb	Ti	Zn
Conc. unit	—	—	—	18.192%	0.003%	0.031%	—

arising from the phosphate group of $FePO_4$.[17] The peak at 531.2 eV (Fig. 3(d)) is attributed to the lattice oxygen of $FePO_4$.[18] The XPS results confirm that the synthesized samples possess the typical peaks of $FePO_4$.

In a control experiment, when the mixture was not elevated to 85 °C for 30 min, the obtained $FePO_4{\cdot}2H_2O$ samples presented flower-like structures, as shown in Fig. 3(e). The size of the synthesized $FePO_4{\cdot}2H_2O$ samples is ~10 μm. It is clear that the flower-like $FePO_4{\cdot}2H_2O$ is dispersed, and the particles are composed of a lot of thin sheets. It is believed that the heat treatment contributed to the process of fusing the thin sheets into the polyhedral structure (Fig. 2(d)). The pickling of precipitate samples by dilute nitric acid is helpful for the improvement in the Fe/P ratio of $FePO_4{\cdot}2H_2O$ samples. Table 3 shows the ICP analysis of synthesized $FePO_4{\cdot}2H_2O$ in the absence of acid washing by dilute nitric acid. It was found that the Fe/P ratio of $FePO_4{\cdot}2H_2O$ samples was 0.93, which was lower than that (1.03) when acid washing was used. The reason may be that dilute nitric acid could react with the impurities (*e.g.*, $Fe(OH)_3$), which would improve the Fe/P ratio of $FePO_4{\cdot}2H_2O$ samples. Therefore, it can be concluded that the reaction temperature and washing process are critical for the synthesis of battery-grade $FePO_4{\cdot}2H_2O$ with a high Fe/P ratio.

In conclusion, high-pressure hydrolyzed precipitates of cobalt–iron alloy acid solution were successfully used for the synthesis of battery-grade ferric phosphate ($FePO_4{\cdot}2H_2O$). The reaction of $FePO_4{\cdot}2H_2O$ was carried out at a pH of 2.57, which will not lead to the precipitation of other impurity elements, such as Ca^{2+}, Zn^{2+} or Ni^{2+}. Therefore, the obtained $FePO_4{\cdot}2H_2O$ samples have high purity. The morphology of battery-grade $FePO_4{\cdot}2H_2O$ is related to the reaction temperature, and the acid washing using dilute nitric acid for the precipitates was demonstrated to be an effective way to increase the Fe/P ratio. The results indicate that the synthesized $FePO_4{\cdot}2H_2O$ samples have a higher Fe/P ratio (1.03) than standard ferric phosphate (0.98–1.02). The results indicate that our technical route in this paper provides an important idea for the resource utilization of industrial solid waste containing iron.

The authors acknowledge China Nonferrous Metals Innovation Institute (Tianjin) Co., Ltd. Technology Development Project (2023KJZX036).

Data availability

The data supporting this article have been included as part of the ESI.†

Conflicts of interest

There are no conflicts to declare.

Notes and references

1 K. Schulze, F. Kullmann, J. M. Weinand and D. Stolten, *Joule*, 2024, **8**, 1936–1957.
2 A. Pommeret, F. Ricci and K. Schubert, *Eur. Econ. Rev.*, 2022, **141**, 103991.
3 C. Xu, Q. Dai, L. Gaines, M. Hu, A. Tukker and B. Steubing, *Commun. Mater.*, 2020, **1**, 99.
4 C. Zhang, Y. Zhong, H. Tu, Z. Yang, G. Chen and X. Zhu, *Ionics*, 2024, **30**, 3819–3829.
5 B. Chen, M. Liu, S. Cao, G. Chen, X. Guo and X. Wang, *Mater. Chem. Phys.*, 2022, **279**, 125750.
6 W. B. Lou, Y. Zhang, Y. Zhang, S. L. Zheng, P. Sun, X. J. Wang, S. Qiao, J. Z. Li, Y. Zhang, D. Y. Liu, M. Wenzel and J. J. Weigand, *J. Alloys Compd.*, 2021, **856**, 158148.
7 M. Wang, Y. Xue, K. Zhang and Y. Zhang, *Electrochim. Acta*, 2011, **56**, 4294–4298.
8 Y. M. Zhu, Z. W. Ruan, S. Z. Tang and V. Thangadurai, *Ionics*, 2014, **20**, 1501–1510.
9 T. Zhao, H. Mahandra, R. Marthi, X. Ji, W. Zhao, S. Chae, M. Traversy, W. Li, F. Yu, L. Li, Y. Choi, A. Ghahreman, Z. W. Zhao, C. Zhang, Y. Kang, Y. Lei and Y. Song, *Chem. Eng. J.*, 2024, **485**, 149923.
10 L. Deng, G. Ma and Q. Chen, *Integr. Ferroelectr.*, 2023, **234**, 67–78.
11 X. Zhang, K. Zhou, D. Zeng, J. Li, Y. Wu, W. Chen and C. Peng, *Bull. Environ. Contam. Toxicol.*, 2022, **109**, 86–94.
12 M. Chen, D. Sukhomlinov, P. Taskinen, J. Hamuyuni, R. M. Michallik, M. Lindgren and A. Jokilaakso, *J. Sustainable Metal*, 2024, **10**, 360–374.
13 Y. Liu, Z. Li, Y. You, X. Zheng and J. Wen, *RSC Adv.*, 2017, **7**, 51281–51289.
14 R. Dedryvère, M. Maccario, L. Croguennec, F. Le Cras, C. Delmas and D. Gonbeau, *Chem. Mater.*, 2008, **20**, 7164–7170.
15 R. Cai, Y. Du, W. Zhang, H. Tan, T. Zeng, X. Huang, H. Yang, C. Chen, H. Liu, J. Zhu, S. Peng, J. Chen, Y. Zhao, H. Wu, Y. Huang, R. Xu, T. M. Lim, Q. Zhang, H. Zhang and Q. Yan, *Chem. – Eur. J.*, 2013, **19**, 1568–1572.
16 T. R. I. Cataldi, G. E. De Benedetto and A. Bianchini, *J. Electroanal. Chem.*, 1998, **448**, 111–117.
17 D. Dedryvère, M. Maccario, L. Croguennec, F. L. Cras, C. Delmas and D. Gonbeau, *Chem. Mater.*, 2008, **20**, 7164–7170.
18 B. Pandit, B. Fraisse, L. Stievano, L. Monconduit and M. T. Sougrati, *Electrochim. Acta*, 2022, **409**, 139997.